Petroleum Science 22 (2025) 1578–1595

Contents lists available at ScienceDirect

Petroleum Science

journal homepage: www.keaipublishing.com/en/journals/petroleum-science

Original Paper

Numerical calculation of bottom hole circulating temperature in wellbore cementing processes with multi-fluid and multi-step

Xu-Ning Wu [a, b], Zheng-Meng Hou [a, *], Zao-Yuan Li [b], Bo Feng [b, c, **], Lin Wu [a, b], Qian-Jun Chen [a], Nan Cai [a, b], Ting-Cong Wei [d]

[a] *Institute of Subsurface Energy Systems, Clausthal University of Technology, Clausthal-Zellerfeld, 38678, Germany*
[b] *National Key Laboratory of Oil and Gas Reservoir Geology and Exploitation, Southwest Petroleum University, Chengdu, 610500, Sichuan, China*
[c] *Petroleum Engineering Technology Institute of Southwest Petroleum Branch, SINOPEC, Deyang, 618000, Sichuan, China*
[d] *School of Civil Engineering and Architecture, Guangxi University, Nanning, 530004, Guangxi, China*

A R T I C L E I N F O

Article history:
Received 2 September 2024
Received in revised form
24 February 2025
Accepted 24 February 2025
Available online 25 February 2025

Edited by Jia-Jia Fei

Keywords:
Cementing processes
Bottom hole circulating temperature
Multi-fluid injection
Transient temperature field

A B S T R A C T

In oil and gas well cementing processes, accurately predicting the bottom hole circulating temperature (BHCT) is critical to ensuring effective zonal isolation. Overestimating the temperature can lead to excessive retardation issues, while underestimation can cause cementing accidents. Current methods for calculating the BHCT of cement slurry typically simplify the cementing processes to a single-fluid circulation and ignore the impact of pre-cementing processes on temperature, leading to significant discrepancies between calculated and actual results. In this study, the wellbore and formation are simplified into a two-dimensional axisymmetric structure, and a mathematical model of the temperature field under multi-fluid and multi-step conditions is established based on the law of energy conservation. The finite volume method was used to discretize the model, and a transient temperature field solver for the entire cementing process was developed, which can numerically calculate the temperature of any fluid at any time, any location. For an actual well example, the temperature distribution of the wellbore and formation after casing running is taken as the initial condition. Numerical calculations were performed sequentially to calculate the temperature fields of circulation flushing, wellbore preparation, and cementing, as well as the BHCT of the cement slurry. The study reveals that during the circulation flushing stage, the maximum temperature point in the wellbore is located at a distance of about 366 m above the bottom of the well. In the wellbore preparation stage, due to static heat exchange, the maximum temperature point gradually shifts to the bottom of the well. The BHCT of cement slurry changes continuously under cementing processes with multi-fluid and multi-step, making it a transient value. The BHCT of the lead slurry and tail slurry are not equal, with the maximum BHCT of the tail slurry being 2.46 °C higher than that of the lead slurry. If circulation flushing and wellbore preparation are not considered, the calculated BHCT of the cement slurry will have errors of +6.8% and −1.9%. The study highlighted that considering thermal effects of all cementing stages, such as circulation flushing and wellbore preparation, in BHCT calculations can help improve prediction accuracy.

1. Introduction

The core objective of cementing processes is to effectively seal the annulus space between the formation and the casing using cement slurry, thereby isolating the oil, gas, and water layers and establishing a safe channel for oil and gas extraction. To ensure the sealing effectiveness of the cement slurry, it is essential to minimize its setting time, enabling the slurry to solidify rapidly after reaching the predetermined depth in the annulus (Bittleston, 1990). This rapid solidification reduces the likelihood of formation fluids entering the cement slurry and enhances the bonding strength between the cement sheath, the formation, and the casing. Accurate prediction of the bottom hole circulating temperature (BHCT)

* Corresponding author.
** Corresponding author.
E-mail addresses: hou@tu-clausthal.de (Z.-M. Hou), fengboswpu@126.com (B. Feng).

https://doi.org/10.1016/j.petsci.2025.02.018
1995-8226/

Nomenclature

Symbols

C_c	Specific heat of fluid in casing, J/(kg·°C)
C_w	Specific heat of casing, J/(kg·°C)
C_a	Specific heat of fluid in annulus, J/(kg·°C)
C_f	Specific heat of formation, J/(kg·°C)
T_c	Temperature of fluid in casing, °C
T_w	Temperature of casing, °C
T_a	Temperature of fluid in annulus, °C
T_{f1}	Temperature of wellbore rock, °C
T_{fi}	Temperature of the i-th ($i \geq 2$) layer in the radial direction inside the formation, °C
v_c	Fluid velocity in casing, m/s
v_a	Fluid velocity in annulus, m/s
h_{ci}	Convective heat transfer coefficient between the casing fluid and the casing inner wall, W/(m^2·°C)
h_{co}	Convective heat transfer coefficient between the annulus fluid and the casing outer wall, W/(m^2·°C)
h_b	Convective heat transfer coefficient between the annulus fluid and the wellbore wall, W/(m^2·°C)
r_{ci}	Casing inner radius, m
r_{co}	Casing outer radius, m
r_b	Wellbore radius, m
r_{f1}	The distance from the central symmetry axis to the wellbore unit center, m
r_{fi}	The distance from the central symmetry axis to the i-th ($i \geq 2$) layer of the formation unit center, m
Q_c	Thermal power generated by the fluid in the casing, W/m
Q_a	Thermal power generated by the fluid in the annulus, W/m
t	Time, s
z	Well depth, m

Greek symbols

ρ_c	Density of fluid in casing, kg/m^3
ρ_w	Density of casing, kg/m^3
ρ_a	Density of fluid in annulus, kg/m^3
ρ_f	Density of formation, kg/m^3
λ_c	Thermal conductivity of fluid in casing, W/(m·°C)
λ_w	Thermal conductivity of casing, W/(m·°C)
λ_a	Thermal conductivity of fluid in annulus, W/(m·°C)
λ_f	Thermal conductivity of formation, W/(m·°C)

of the cement slurry is crucial for ensuring the safety of the cementing processes and improving cementing quality (Chen and Novotny, 2003; Guillot et al., 1993). However, since the cement slurry forms a unified whole with the formation and casing after setting, it is challenging to directly measure the actual temperature of the cement slurry during the processes. The setting time of the cement slurry is determined by its formulation, and BHCT, as one of the key parameters in formulation design (Beirute, 1991), directly influences the selection and dosage of chemical additives.

Currently, the main methods for predicting cement slurry BHCT include the American Petroleum Institute (API) calculation method and empirical coefficient methods based on it, which consider well depth and geothermal gradient. However, these methods generally only provide a rough estimate of the BHCT range. To prevent premature setting of the cement slurry before it is fully displaced into the annulus, cementing engineers often adopt conservative predictions, leading to a common issue of overestimated BHCT in actual processes (Davies et al., 1994; Honore et al., 1993). Sump and Williams (1973) developed a numerical solution program to calculate cement slurry BHCT and corrected its pumpable time based on the heat release characteristics of cement hydration. The research indicates that there can be a significant discrepancy, up to 30 °C, between temperatures calculated using the API method or previous models and measured temperatures. This study has the potential to shorten the cement slurry setting time in the well by at least 30 min. Bittleston (1990) constructed a two-dimensional transient model of the wellbore-formation system and used finite difference numerical methods for the solution. His research suggests that the highest fluid temperature occurs at a certain distance above the annulus, emphasizing that the temperature measured at the well bottom should not be used as the design temperature for cement slurry. He also highlighted the need to consider the formation temperature distribution at the start of the cementing processes to reduce its impact on BHCT predictions. Guillot et al. (1993) developed a one-dimensional transient model of the wellbore-formation system and used the Laplace transform method for numerical solutions, obtaining temperature variation curves for cement slurry circulation and well shut-in. Compared with the API method and measured values, Guillot's model predictions are more reliable, especially when the well depth exceeds 4600 m, where the API method's prediction errors are larger, with an average error of about 10 °C. Chen and Novotny (2003) based on the law of conservation of mass and heat transfer theory, established a cement slurry circulation temperature model and used the finite difference method to solve for the temperature distribution within the wellbore and formation. His research pointed out that the highest temperature in the wellbore is located at a distance of about one-quarter to one-third of the well depth from the bottom.

It is evident that using wellbore temperature field models to predict cement slurry BHCT is a more precise technical approach. This method can comprehensively consider various sensitive factors and is highly consistent with the temperature distribution and evolution patterns observed in actual cementing processes. Research methods for wellbore temperature field models are mainly categorized into three types: analytical models, transient numerical calculation methods, and Computational Fluid Dynamics (CFD) simulation methods. Analytical models usually assume stable heat transfer within the wellbore and transient heat conduction within the formation. By utilizing temperature distribution functions proposed by different researchers (Kabir et al., 1996), the wellbore temperature can be described as a function of well depth and time. Transient numerical calculation methods establish thermal equilibrium equations for various regions using partial differential equations, and the temperature changes over time within the wellbore and formation are calculated through numerical solutions (Yang et al., 2019; Zhang et al., 2018). With the development of computer hardware and reservoir technology in this century, CFD simulation software has integrated mathematical models of temperature fields, primarily using the finite volume method to solve temperature variations during fluid flow, providing a novel computational approach (Wu and Han, 2009).

The temperature variation of fluids within a wellbore at different circulation times can be solved using analytical models. Moss and White (1959) assumed a quasi-steady-state for fluid temperature in the wellbore, disregarding the time-dependent temperature effects, and solved the wellbore temperature distribution through spatial discretization. Ramey (1962) addressed the heat exchange issue when hot or cold fluids enter the wellbore, assuming radial heat flow from the formation into the wellbore, with the thermal resistance within the wellbore being much smaller than that of the formation. He proposed a quasi-steady-state temperature distribution model and defined the calculation method for the overall heat transfer coefficient, laying the foundation for subsequent analytical model research. Holmes and Swift (1970) assumed steady-state linear heat transfer between the formation and the annulus drilling fluid, constructing an analytical expression for the wellbore fluid temperature under the premise of neglecting axial heat conduction. When fluid circulation time is long, the model's results are close to those of the Raymond model (Raymond, 1969). Arnold (1990) assumed a quasi-steady-state for wellbore temperature and a transient formation temperature, neglecting heat sources like viscous dissipation and the effects of the casing, and constructed a wellbore-formation thermal equilibrium equation set, providing analytical solutions for fluid temperature distribution in both the annulus and the casing. Kabir et al. (1996) argued that to calculate changes in fluid density and viscosity within the wellbore, one must first determine the temperature distribution, and he developed a quasi-steady-state analytical model for wellbore fluid temperature, which is suitable for calculating the temperature of reverse-injected fluids during well workovers. However, current analytical models for wellbore temperature fields are mostly based on drilling processes, making them more applicable to single-fluid long-duration circulation where temperature distribution tends to stabilize, with limited applicability to cementing processes involving multiple fluids.

Cementing processes involve various fluids, some of which are used in small quantities and cannot form a fluid circulation. The temperature, volume, and injection rate of each fluid change over time, altering the flow and heat transfer of the fluids within the wellbore. Compared to analytical models, transient temperature field models combined with numerical solution methods can better describe the transient heat exchange mechanisms between different regions of the wellbore and formation. Edwardson et al. (1962) proposed a one-dimensional transient temperature field model based on heat transfer principles and solved it using numerical methods, obtaining temperature disturbance curves in the surrounding formation for different circulation times. Raymond (1969), based on Bird's heat flow equation (Bird et al., 1960), constructed both quasi-steady-state and transient temperature field models, finding that after 4 h of drilling fluid circulation, the results from both models were nearly identical, laying the foundation for the development of transient models. Keller et al. (1973) further expanded Raymond's research by constructing a two-dimensional transient model that considered the casing temperature and additional heat sources such as viscous dissipation energy, and solved it using the finite difference method. Yang et al. (2015, 2017) developed a transient heat transfer model that could be used to calculate temperature changes in the wellbore fluids and formation under well kick conditions and considering drill string assembly and casing program. Wang et al. (2024) established a temperature and pressure coupled transient heat transfer model during the drilling fluid circulation, and theoretically proved that under quasi-steady state, the downhole temperature increases linearly with the inlet temperature. Zhang et al. (2024) analyzed the effect of gas influx on the wellbore temperature field during managed pressure drilling. However, current research on transient temperature fields has not fully considered the simultaneous presence of multiple fluids with different flow regimes and thermal properties during cementing processes.

CFD simulation software, which combines fluid mechanics and heat transfer principles, can be used to simulate fluid flow and transient temperature distribution within the wellbore. Wang et al. (2019), addressing the BHCT issue in offshore cementing processes, constructed a two-dimensional simulation model using ANSYS software. Utilizing the momentum and heat-solving modules, he simulated the interface and temperature changes during the cement slurry displacement process. Wang et al. (2021) considered the cementing plug in the geometric model, simulated the temperature distribution of the cement slurry and formation, and indicated that the radial influence range of fluid on the formation temperature around the well bottom during cementing processes was about 0.5 m. Abdelhafiz et al. (2021), focusing on the fluid circulation temperature calculation during drilling, established a three-dimensional simulation model using ANSYS software and compared it with the results from the two-dimensional model, finding little difference between the two, with a maximum temperature difference of only 0.23 °C. Although CFD simulations can calculate fluid temperatures within the wellbore, the heat transfer rates in the software are difficult to adjust, and the numerical solving efficiency is lower compared to transient model programs (Abdelhafiz et al., 2021).

Previous studies on BHCT of cement slurry often overlooked the impact of pre-cementing processes on the calculation results. Although Bittleston (1990) acknowledged the importance of considering the formation temperature distribution before cement slurry injection, subsequent research did not carry out detailed computational analysis. Cementing processes typically include circulation flushing, wellbore preparation, and cement slurry injection of. Before injecting cement slurry, various types of pre-flush fluids are also introduced. In previous studies, methods used to calculate the circulation temperature of drilling fluids did not account for the impact of these preceding steps on the temperature distribution within the wellbore and the surrounding formation. Instead, they assumed that the temperature distribution of the wellbore and formation at the time of cement slurry injection was the same as that of the original formation. This assumption led to significant deviations in the calculation results. It has been widely observed in the cementing industry that the downhole drilling fluid circulation temperature obtained from Measurement While Drilling (MWD) and the static temperature of the drilling fluid obtained after drilling completion differ from the actual BHCT of the cement slurry. Due to the lack of real-time temperature calculations for the cement slurry from injection to the end of flow, engineers must rely on API methods and regional experience to make rough estimates when designing cement slurry formulations and determining thickening test temperatures. To prevent premature solidification of the cement slurry, the cementing processes has become extremely cautious, leading to issues such as over-retardation of the cement slurry and annulus gas migration, problems that have long plagued cementing processes (Garcia and Clark, 1976; Guo et al., 2014, 2019), as highlighted by the report on the Deepwater Horizon incident (Mangadlao et al., 2015).

This study establishes a transient temperature field mathematical model based on the physical processes of various cementing stages and the heat transfer characteristics between fluids, the casing, and the formation. The model employs the finite volume method to numerically solve the partial differential equations. The study calculates the fluid locations within the wellbore during different stages and the temperature distribution across the wellbore-formation regions, determining the BHCT of the cement slurry and analyzing the effect of different initial temperatures on the slurry temperature. The innovation of this research lies in the first-time calculation and analysis of temperature changes in the wellbore and formation throughout the entire cementing processes, including the temperature evolution of drilling fluid, spacer fluids, cement slurry, and displacement fluids during their flow. The results of this study can provide guidance for improving cementing procedures, cement slurry formulation, and thickening test experiments.

2. Calculation model of cement slurry BHCT during the whole cementing processes

2.1. Physical model

According to the actual cementing processes, a typical cementing job is divided into three continuous stages: circulation flushing, wellbore preparation, and cement slurry injection, as illustrated in Fig. 1. The circulation flushing process begins after the casing running. The wellbore is filled with drilling fluid, and pumping starts to inject the fluid, gradually establishing a stable single-fluid circulation. During the wellbore preparation stage, the drilling fluid remains static, allowing the temperature throughout the well to gradually return to equilibrium. The cement slurry injection stage involves the sequential injection and displacement of various fluids, each with different temperatures and flow rates. During this process, the speed, location, and heat transfer rate of the fluids in casing and annulus continuously change, and a stable fluid circulation cannot be established.

Throughout the entire physical process, heat transfer within the wellbore can be categorized into two types: heat transfer during fluid flow and heat transfer during fluid stagnation. When fluid flows within the wellbore, it is injected at a certain temperature from the wellhead, flows downward along the inner wall of the casing, reaches the bottom of the well, and then flows back into the annulus space, moving upward along the annulus space between the casing and the surrounding rocks. During this process, the fluid temperature is primarily influenced by two factors: axial advective heat transfer and radial convective heat transfer between the fluid and the wellbore wall (Abdelhafiz et al., 2020). After the fluid circulates for a period of time, the wellbore preparation stage begins. The fluid movement gradually stops, and the fluid in the wellbore enters a static state. Due to the fluid flow of circulation stage, the axial temperature distribution in the wellbore and surrounding areas changes significantly compared to the original temperature or the initial stable state, resulting in a noticeable radial temperature difference between the wellbore and the surrounding rocks. According to the second law of thermodynamics, this temperature difference drives heat transfer, which occurs mainly through conduction. During the fluid static period, since there is minimal variation in fluid density and temperature along the axial direction, heat transfer due to natural convection can be neglected.

In cement slurry injection process, field engineers typically focus on the BHCT of the cement slurry, which represents the maximum temperature near the bottom of the well. Although the casing and cement sheath can influence the temperature distribution, this impact is mostly concentrated in the upper sections of the system, with minimal effect on the bottom hole temperature. Therefore, when establishing a physical model, it is possible to simplify the wellbore and surrounding rocks. The simplified physical model is shown in Fig. 2, assuming that the surrounding rock is a homogeneous single-layer rock. The model mainly considers the radial convection heat transfer between the formation and the annulus fluid, the annulus fluid and the casing string, the casing string and the casing fluid, the flow pattern and location of multiple fluids, and the axial advection heat transfer.

Assuming the casing is centered and the materials in all parts of the wellbore are uniform, the physical structure can be simplified into a two-dimensional axisymmetric geometric structure. The temperature field of the wellbore and surrounding rock can be divided into four regions, as shown in Fig. 3. The first region is the fluid inside the casing, with a temperature denoted as T_c; the second region is the casing, with a temperature T_w; the third region is the annulus fluid, with a temperature T_a; and the fourth region is the formation, with a temperature T_f. This study primarily focuses on the thermal energy of the fluids, and therefore simplifies the momentum and mass equations by assuming uniform fluid flow velocities and constant density in both the casing and annulus. The

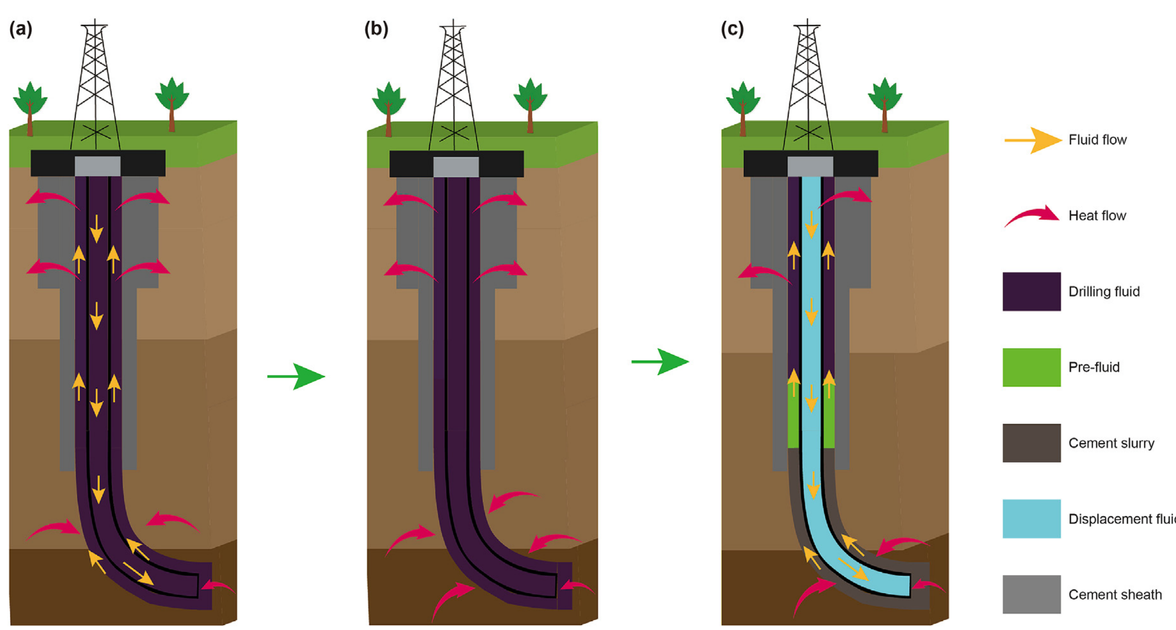

Fig. 1. Conventional cementing processes. (**a**) circulation flushing, (**b**) wellbore preparation, (**c**) cement slurry injection.

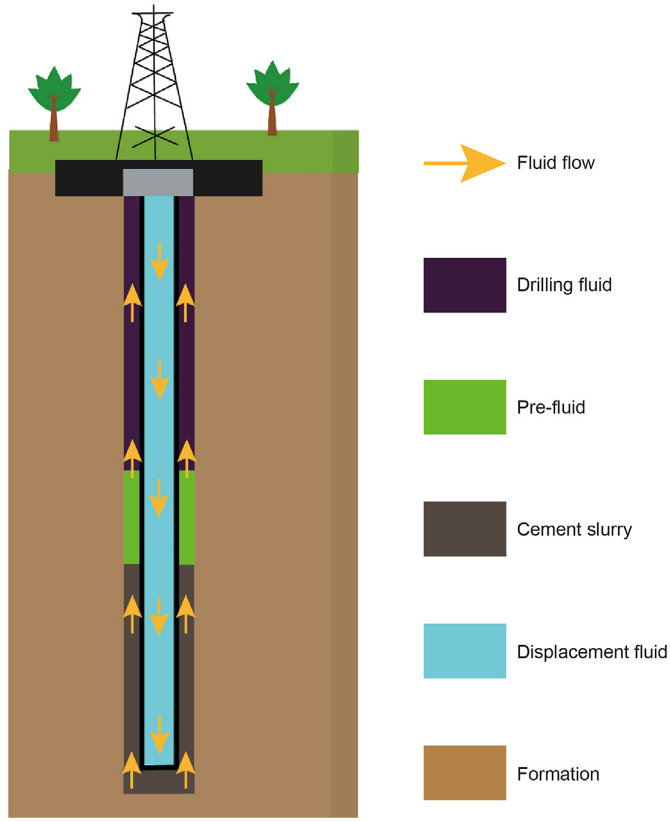

Fig. 2. Simplified schematic of the physical model.

coordinate z represents the axial direction of the wellbore, r represents the radial direction, and t represents time.

2.2. Cementing fluid flow temperature model

Based on the equations for heat conduction and heat convection, heat balance equations are established for each of the four regions. The derivation process of the temperature control equation is briefly illustrated using the heat balance equation of the fluid within the casing as an example.

The wellbore is discretized along the z-axis into uniform volumetric elements of length δz, as shown in Fig. 4.

Axial fluid flow in the wellbore induces heat transfer. The heat entering a volumetric element during time interval dt is modeled using an upwind scheme for fluid flow as:

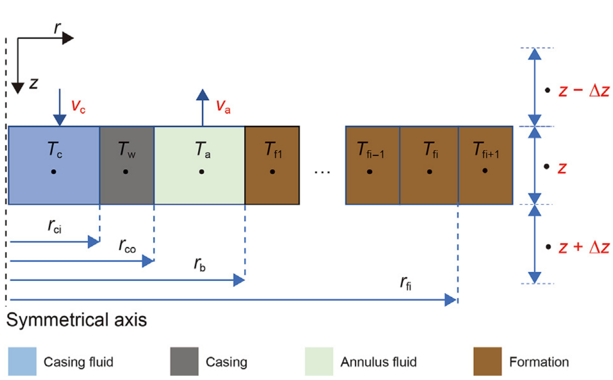

Fig. 3. Area division schematic of temperature field system.

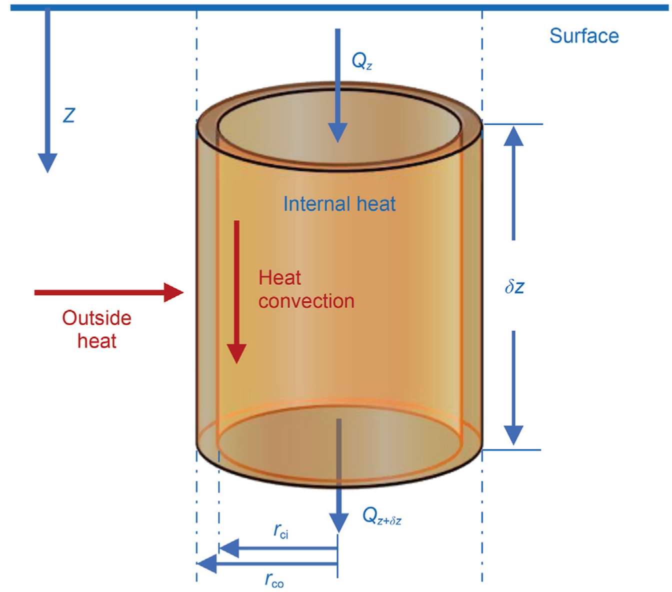

Fig. 4. The fluid volumetric element within the casing.

$$\mathrm{d}Q_1 = Q_z - Q_{z+\delta z} = \pi r_{\mathrm{ci}}^2 \rho_{\mathrm{c}} v_{\mathrm{c}} C_{\mathrm{c}} \left[T_{\mathrm{c}(z-\delta z)} - T_{\mathrm{c}z} \right] \mathrm{d}t \tag{1}$$

In the radial direction, the convective heat transfer between the fluid and the casing during time interval dt is:

$$\mathrm{d}Q_2 = 2\pi r_{\mathrm{ci}} h_{\mathrm{ci}} (T_{\mathrm{w}} - T_{\mathrm{c}}) \delta z \mathrm{d}t \tag{2}$$

The energy generated by viscous dissipation due to frictional pressure drop during time interval dt is:

$$\mathrm{d}W = Q_{\mathrm{c}} \delta z \mathrm{d}t \tag{3}$$

The total accumulated energy change within the volumetric element during time interval dt is:

$$\mathrm{d}E = \rho_{\mathrm{c}} C_{\mathrm{c}} \frac{\partial T_{\mathrm{c}}}{\partial t} \pi r_{\mathrm{ci}}^2 \delta z \mathrm{d}t \tag{4}$$

The term Q_z in Eq. (1), along with dQ_2 in Eq. (2) and dW in Eq. (3), represents the energy entering the volumetric element, while $Q_{z+\delta z}$ in Eq. (1) represents the energy leaving the element. According to the first law of thermodynamics, dQ + dW = dE. Upon rearrangement, the energy balance equation for the fluid inside the casing is derived as:

$$\rho_{\mathrm{c}} C_{\mathrm{c}} \frac{\partial T_{\mathrm{c}}}{\partial t} = \rho_{\mathrm{c}} C_{\mathrm{c}} v_{\mathrm{c}} \frac{\partial T_{\mathrm{c}}}{\partial z} + \frac{2h_{\mathrm{ci}}(T_{\mathrm{w}} - T_{\mathrm{c}})}{r_{\mathrm{ci}}} + \frac{Q_{\mathrm{c}}}{\pi r_{\mathrm{ci}}^2} \tag{5}$$

Energy balance equations for other components of the system are similarly derived using the finite volume method, as discussed in (Raymond, 1969), (Keller et al., 1973), (Marshall and Bentsen, 1982), and (Yang et al., 2019). Readers interested in further details are encouraged to refer to the original articles.

The temperature T_{w} of the casing is mainly influenced by convective heat transfer between the casing and both the fluid inside the casing and the annulus fluid, as well as axial conductive heat transfer along the casing. The heat balance equation for the casing is:

$$\rho_w C_w \frac{\partial T_w}{\partial t} = \frac{2r_{co}h_{co}}{r_{co}^2 - r_{ci}^2}(T_a - T_w) + \frac{2r_{ci}h_{ci}}{r_{co}^2 - r_{ci}^2}(T_c - T_w) + \lambda_w \frac{\partial^2 T_w}{\partial z^2} \tag{6}$$

In Eq. (6), the left side represents the accumulation of heat in the casing over time. The first term on the right side represents the radial convective heat transfer between the casing and the annulus fluid. The second term accounts for radial convective heat transfer between the casing and the fluid inside the casing, and the final term represents axial conductive heat transfer along the casing.

The temperature T_a of the annulus fluid is primarily influenced by convective heat transfer between the annulus fluid and both the casing and the formation rock, as well as advective heat transfer as the fluid flows upward. The heat balance equation for the annulus fluid is:

$$\rho_a C_a \frac{\partial T_a}{\partial t} = \rho_a C_a v_a \frac{\partial T_a}{\partial z} + \frac{2r_b h_b \left(T_{f1} - T_a\right)}{r_b^2 - r_{co}^2} + \frac{2r_{co}h_{co}(T_w - T_a)}{r_b^2 - r_{co}^2} + \frac{Q_a}{\pi\left(r_b^2 - r_{co}^2\right)} \tag{7}$$

In Eq. (7), the left side represents the accumulation of heat in the annulus fluid over time. The first term on the right side represents heat transfer via advection as the fluid moves upward. The second term accounts for radial convective heat transfer between the wellbore wall and the annulus fluid. The third term represents radial convective heat transfer between the casing and the annulus fluid, and the final term accounts for heat generated by friction as the fluid flows within the annulus.

The temperature T_{f1} of the wellbore wall is the first radial layer in contact with the annulus fluid. This temperature is primarily determined by radial convective heat transfer between the wellbore wall and the annulus fluid, as well as conductive heat transfer radially and axially through the wellbore wall and the surrounding rock. The heat balance equation for the wellbore wall is:

$$\rho_f C_f \left(r_{f1}^2 - r_b^2\right) \frac{\partial T_{f1}}{\partial t} = \frac{2r_b \lambda_f h_b \left(T_a - T_{f1}\right)}{\lambda_f + h_b r_b \ln\left(\left(r_b + r_{f1}\right)/2r_b\right)} + \frac{2\lambda_f \left(T_{f2} - T_{f1}\right)}{\ln\left(\left(r_{f2} + r_{f1}\right)/\left(r_b + r_{f1}\right)\right)} + \left(r_{f1}^2 - r_b^2\right)\lambda_f \frac{\partial^2 T_{f1}}{\partial^2 z} \tag{8}$$

In Eq. (8), the left side represents the accumulation of heat in the wellbore wall over time. The first term on the right side represents radial convective heat transfer between the wellbore wall and the annulus fluid. The second term accounts for radial conductive heat transfer between the wellbore wall and the adjacent formation, and the final term represents axial conductive heat transfer along the wellbore wall.

The temperature T_{fi} within the surrounding rock is primarily determined by radial and axial conductive heat transfer within the surrounding rock. The heat balance equation for the surrounding rock (where $i \geq 2$):

$$\rho_f C_f \left(r_{fi}^2 - r_{fi-1}^2\right) \frac{\partial T_{fi}}{\partial t} = \frac{2\lambda_f \left(T_{fi-1} - T_{fi}\right)}{\ln\left(\left(r_{fi} + r_{fi-1}\right)/\left(r_{fi-2} + r_{fi-1}\right)\right)} + \frac{2\lambda_f \left(T_{fi+1} - T_{fi}\right)}{\ln\left(\left(r_{fi} + r_{fi+1}\right)/\left(r_{fi} + r_{fi-1}\right)\right)} + \left(r_{fi}^2 - r_{fi-1}^2\right)\lambda_f \frac{\partial^2 T_{fi}}{\partial^2 z} \tag{9}$$

In Eq. (9), the left side represents the accumulation of heat within the surrounding rock over time. The first term on the right side represents radial conductive heat transfer toward the wellbore, the second term represents radial conductive heat transfer away from the wellbore, and the final term accounts for axial conductive heat transfer within the surrounding rock.

2.3. Cementing fluid static temperature model

When the fluid within the wellbore is stationary, heat exchange within the system primarily occurs through heat conduction. Referring to the derivations of Yang et al. (2015) and Abdelhafiz et al. (2021), heat balance equations are established for each of the four regions, as shown in Fig. 3.

The first PDE calculates the temperature T_c of the stationary fluid inside the casing. Due to the significantly larger radial temperature gradient compared to the axial one, and the relatively low thermal conductivity of the fluid, axial heat conduction can be neglected. During the wellbore preparation stage, the fluid is stationary, and the drilling fluid has no axial density differences, so the effects of natural convection can also be ignored, as shown in Fig. 1(b). The heat balance equation for the stationary fluid inside the casing is:

$$\rho_c C_c r_{ci}^2 \frac{\partial T_c}{\partial t} = \frac{2(T_c - T_w)}{\ln(2r_{ci}/r_{ci})/\lambda_c + \ln((r_{co} + r_{ci})/2r_{ci})/\lambda_w} \tag{10}$$

In Eq. (10), the left side represents the heat accumulation of the fluid over time. The right side represents the heat conduction within the fluid in the radial direction and the heat transferred between the fluid and the casing.

The second PDE calculates the temperature T_w of the casing. The heat balance equation for the casing is:

$$\rho_w C_w \left(r_{co}^2 - r_{ci}^2\right) \frac{\partial T_w}{\partial t} = \frac{2(T_c - T_w)}{\ln(2r_{ci}/r_{ci})/\lambda_c + \ln((r_{co}+r_{ci})/2r_{ci})/\lambda_w} - \frac{2(T_w - T_a)}{\ln(2r_{co}/(r_{co}+r_{ci}))/\lambda_w + \ln((r_{co}+r_b)/2r_{co})/\lambda_a} - \lambda_w \left(r_{co}^2 - r_{ci}^2\right) \frac{\partial^2 T_w}{\partial^2 z} \tag{11}$$

In Eq. (11), the left side represents the heat accumulation of the casing over time. The first term on the right side represents the heat transferred by conduction between the casing and the fluid inside the casing, the second term represents the heat transferred by conduction between the casing and the annulus fluid, and the last term represents the heat conducted axially along the casing.

The third PDE calculates the temperature T_a of the annulus fluid. The heat balance equation for the stationary fluid inside the annulus is:

$$\rho_a C_a\left(r_b^2-r_{co}^2\right)\frac{\partial T_a}{\partial t}=\frac{2(T_w-T_a)}{\ln(2r_{co}/(r_{co}+r_{ci}))/\lambda_w+\ln((r_b+r_{co})/2r_{co})/\lambda_a}-\frac{2\left(T_a-T_{f1}\right)}{\ln(2r_b/(r_{co}+r_b))\Big/\lambda_a+\ln\left(\left(r_{f1}+r_b\right)\Big/2r_b\right)\Big/\lambda_f} \tag{12}$$

In Eq. (12), the left side represents the heat accumulation of the annulus fluid over time. The first term on the right side represents the heat transferred by conduction between the annulus fluid and the casing, and the second term represents the heat transferred by conduction between the annulus fluid and the wellbore wall.

The fourth PDE calculates the temperature T_{f1} of the wellbore wall. The heat balance equation for the wellbore wall is:

$$\rho_f C_f\left(r_{f1}^2-r_b^2\right)\frac{\partial T_{f1}}{\partial t}=\frac{2\left(T_a-T_{f1}\right)}{\ln(2r_b/(r_{co}+r_b))\Big/\lambda_a+\ln\left(\left(r_{f1}+r_b\right)\Big/2r_b\right)\Big/\lambda_f}-\frac{2\left(T_{f1}-T_{f2}\right)}{\ln\left(r_{f2}+r_{f1}\Big/\left(r_{fb}+r_{f1}\right)\right)\Big/\lambda_3}+\lambda_f\left(r_{f1}^2-r_b^2\right)\frac{\partial^2 T_{f1}}{\partial^2 z} \tag{13}$$

In Eq. (13), the left side represents the heat accumulation of the wellbore wall over time. The first term on the right side represents the heat transferred by conduction in the radial direction between the wellbore wall and the annulus fluid, the second term represents the heat transferred by conduction in the radial direction between the wellbore wall and the adjacent formation, and the last term represents the heat conducted axially along the wellbore wall.

Since heat transfer within the formation is always by conduction and is unaffected by the fluid velocity in the wellbore, the temperature within the formation can still be represented by Eq. (9) when the fluid in the wellbore is stationary.

2.4. Fluid location calculation method

Cementing processes involve the injection and displacement of multiple fluids, as shown in Fig. 1. Spacer fluids, cement slurry, and displacement fluids each have their own thermal and rheological properties, resulting in different heat transfer rates between the fluid and the casing's inner wall, the casing's outer wall, and the wellbore wall. Therefore, it is necessary to calculate the location of each fluid in the wellbore in real time. The method for calculating fluid location is as follows:

(1) When a fluid satisfies the condition $t_{in}\cdot v_c \le L$, the fluid remains entirely within the casing. The depth distribution of the fluid at this time extends from the wellhead to a depth h, where $h = t_{in}\cdot v_c$ represents the fluid's flow distance. If another fluid has already been injected into the casing behind it, the depth distribution of the preceding fluid ranges from the front-end depth of the following fluid to h.

(2) When a fluid satisfies the condition $t_{in}\cdot v_c > L$, the front end of the fluid has entered the annulus. The corresponding depth of the fluid's front end is $L-\left(t_{in}-\frac{L}{v_c}\right)v_a$. If part of the fluid is within the casing and part is in the annulus, the depth distribution in the casing ranges from the front-end depth of the following fluid to the bottom of the well, while the depth distribution in the annulus ranges from the fluid's front-end depth to the bottom of the well. If the fluid is entirely within the annulus, the depth distribution extends from the fluid's front-end depth to the front-end depth of the following fluid.

2.5. Initial and boundary conditions

To solve the cementing temperature field model, it is necessary to set initial and boundary conditions. Prior to the circulation flushing process such as logging and casing installation cause the fluid in the wellbore to remain stationary for an extended period, allowing the temperature of the wellbore and the surrounding formation to gradually return to equilibrium. Therefore, it can be assumed that the temperature distribution within the wellbore and the formation is consistent with the original formation temperature. The initial conditions for solving the model are represented by Eq. (14).

$$T_c(z,t=0)=T_w(z,t=0)=T_a(z,t=0)=T_f(z,t=0)=T_s+Gz \tag{14}$$

The injection temperature of each fluid can be measured using instruments.

$$T_c(z=0,t)=T_{in} \tag{15}$$

The fluid mixes at the wellbore bottom, leading to equal temperatures between the fluid inside the casing and in the annulus.

$$T_c(z=H)=T_a(z=H) \tag{16}$$

It is generally accepted that the influence of the wellbore fluid on the temperature of the adjacent formation has a limited range. If the radius of the affected zone in the surrounding formation is r_{ei}, then beyond this range, the temperature distribution of the formation is assumed to be consistent with the original formation temperature, as shown in Eq. (17).

$$T_f(r\to r_{ei},z,t)=T_s+Gz \tag{17}$$

The central axis of symmetry, the bottom boundary of the formation, as well as the top and bottom of the casing, are assumed to be adiabatic boundaries.

2.6. Numerical solution of partial differential equations

The solving of PDEs is typically complex and often requires numerical methods via computer programming. In this section, the wellbore and the surrounding formation are simplified using a two-dimensional axisymmetric structure and spatial discretization. The radial direction of the wellbore and formation is refined to facilitate analysis of temperature variations in the boundary layers. The finite volume method (FVM) is used in its explicit form to discretize the PDEs, converting them into algebraic equations suitable for numerical solutions. The FVM is directly based on the integral form of conservation laws within control volumes, which ensures strict conservation of mass, energy, and other properties. In the calculation of the cement slurry BHCT, energy conservation is particularly crucial, and FVM inherently satisfies this requirement. By applying energy conservation to boundary control volumes, FVM facilitates the calculation of heat transfer between the wellbore and the external environment. FVM also exhibits high stability when handling convection and diffusion terms, especially in the presence of strong convection phenomena. During wellbore circulation and cement injection processes, where thermal convection is significant, the numerical stability of FVM ensures the reasonableness and accuracy of the temperature field. In the Fluent solver, the Coupled algorithm is employed to enhance both stability and accuracy. This algorithm solves the momentum and continuity equations simultaneously. By discretizing the pressure gradient term in the momentum equation and the mass flux at the surface implicitly, a fully implicit solution is achieved. To maintain accuracy, the precision of each iteration is set to 10^{-15}. Additionally, a time step of 1 s is used to minimize the cumulative error generated by the iterations.

2.6.1. Spatial discretization

Fig. 5 illustrates the spatial discretization scheme for the wellbore and formation. The left side shows the horizontal section view, while the right side shows the axial section view. The fluid inside the casing, the casing string, and the annulus fluid are discretized in one-dimensional space along the axial direction, while the formation is discretized in two-dimensional space, both axially and radially. Here, z and r represent the axial and radial directions, respectively. The temperature at different locations is represented by i and j, which denote the radial and axial grid points, respectively.

2.6.2. Fluid flow conditions

For numerical solutions under fluid flow conditions within the wellbore, the convective heat transfer coefficient must first be calculated. The equation for the convective heat transfer coefficient is derived from Petukhov (1970).

$$h = \frac{Nu\lambda}{D} \tag{18}$$

$$Nu = \frac{(f/8)RePr}{1.07 + 12.7(f/8)^{1/2}\left(Pr^{2/3} - 1\right)} \tag{19}$$

$$f = (1.82\ln Re - 1.64)^{-2} \tag{20}$$

Based on Fig. 5, the discretization process for Eqs. (5)–(9) is performed. In these equations, the superscript 1 denotes the next time step, and the superscript 0 represents the current time step.

The heat balance equation for the fluid inside the casing is discretized into Eq. (21).

$$T_{1,j}^1 = T_{1,j}^0 + \frac{v_c\Delta t}{\Delta z}\left(T_{1,j-1}^0 - T_{1,j}^0\right) + \frac{2h_{ci}\Delta t}{r_{ci}\rho_1 C_1}\left(T_{2,j}^0 - T_{1,j}^0\right) + \frac{Q_c\Delta t}{\pi r_{ci}^2\rho_1 C_1} \tag{21}$$

The heat balance equation for the casing is discretized into Eq. (22).

$$T_{2,j}^1 = T_{2,j}^0 + \frac{2r_{co}h_{co}\Delta t}{\rho_2 C_2\left(r_{co}^2 - r_{ci}^2\right)}\left(T_{3,j}^0 - T_{2,j}^0\right) + \frac{2r_{ci}h_{ci}\Delta t}{\rho_2 C_2\left(r_{co}^2 - r_{ci}^2\right)}\left(T_{1,j}^0 - T_{2,j}^0\right) + \frac{\lambda_2\Delta t}{\rho_2 C_2\Delta z}\left(T_{2,j+1}^0 - 2T_{2,j}^0 + T_{2,j-1}^0\right) \tag{22}$$

The heat balance equation for the annulus fluid is discretized into Eq. (23).

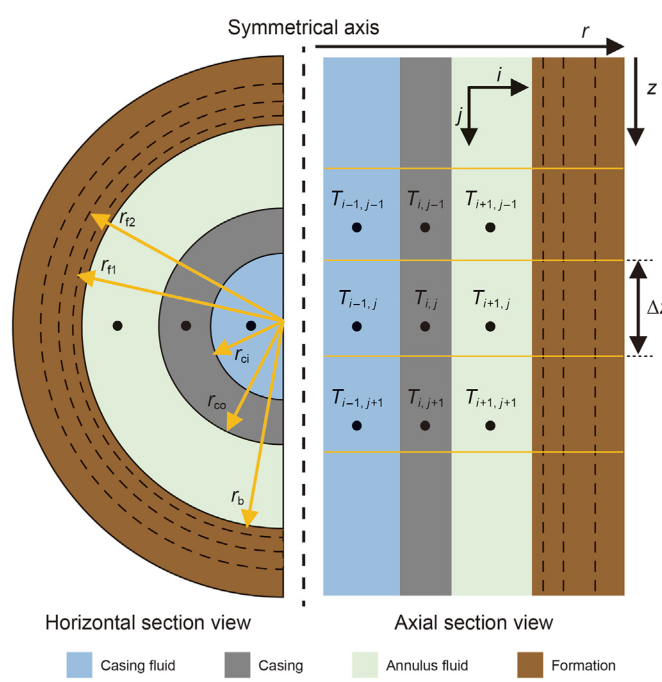

Fig. 5. Schematic of spatial discretization for the wellbore and formation (left: horizontal section view, right: axial section view).

$$T_{3,j}^{1}=T_{3,j}^{0}+\frac{v_a\Delta t}{\Delta z}\left(T_{3,j+1}^{0}-T_{3,j}^{0}\right)+\frac{2r_bh_b\Delta t}{\rho_1C_1\left(r_b^2-r_{co}^2\right)}\left(T_{4,j}^{0}-T_{3,j}^{0}\right)+\frac{2r_{co}h_{co}\Delta t}{\rho_1C_1\left(r_b^2-r_{co}^2\right)}\left(T_{2,j}^{0}-T_{3,j}^{0}\right)+\frac{Q_a\Delta t}{\pi\rho_1C_1\left(r_b^2-r_{co}^2\right)} \tag{23}$$

The heat balance equation for the wellbore wall is discretized into Eq. (24).

$$T_{4,j}^{1}=T_{4,j}^{0}+\frac{2r_b\lambda_3h_b\Delta t\left(T_{3,j}^{0}-T_{4,j}^{0}\right)}{\rho_3C_3\left(r_{f1}^2-r_b^2\right)\left[\lambda_3+h_br_b\ln\left(\left(r_b+r_{f1}\right)/2r_b\right)\right]}+\frac{2\lambda_3\Delta t\left(T_{5,j}^{0}-T_{4,j}^{0}\right)}{\rho_3C_3\left(r_{f1}^2-r_b^2\right)\ln\left(\left(r_{f2}+r_{f1}\right)/\left(r_b+r_{f1}\right)\right)}+\frac{\lambda_3\Delta t}{\rho_3C_3\Delta z^2}\left(T_{4,j+1}^{0}-2T_{4,j}^{0}+T_{4,j-1}^{0}\right) \tag{24}$$

Finally, the heat balance equation for the units within the formation is discretized into Eq. (25).

$$T_{i,j}^{1}=T_{i,j}^{0}+\frac{2\lambda_3\Delta t\left(T_{i-1,j}^{0}-T_{i,j}^{0}\right)}{\rho_3C_3\left(r_{fi}^2-r_{fi-1}^2\right)\ln\left(\left(r_{fi}+r_{fi-1}\right)/\left(r_{fi-2}+r_{fi-1}\right)\right)}+\frac{2\lambda_3\Delta t\left(T_{5,j}^{0}-T_{4,j}^{0}\right)}{\rho_3C_3\left(r_{fi}^2-r_{fi-1}^2\right)\ln\left(\left(r_{fi}+r_{fi-1}\right)/\left(r_{fi-2}+r_{fi-1}\right)\right)}+\frac{\lambda_3\Delta t}{\rho_3C_3\Delta z^2}\left(T_{i,j+1}^{0}-2T_{i,j}^{0}+T_{i,j-1}^{0}\right) \tag{25}$$

2.6.3. Fluid static conditions

For the static fluid conditions in the wellbore, the heat balance equations (Eqs. (10)–(13)) are discretized according to Fig. 5. The discretization method is the same as for the heat balance equations under fluid flow conditions.

The discretized form of the heat balance equation for the fluid inside the casing is:

$$T_{1,j}^{1}=T_{1,j}^{0}+\frac{2\Delta t\left(T_{1,j}^{0}-T_{2,j}^{0}\right)}{\rho_1C_1r_{ci}^2[\ln(2r_{ci}/r_{ci})/\lambda_1+\ln((r_{co}+r_{ci})/2r_{ci})/\lambda_2]} \tag{26}$$

The discretized form of the heat balance equation for the casing is:

$$T_{2,j}^{1}=T_{2,j}^{0}+\frac{2\Delta t\left(T_{1,j}^{0}-T_{2,j}^{0}\right)}{\rho_2C_2\left(r_{co}^2-r_{ci}^2\right)[\ln(2r_{ci}/r_{ci})/\lambda_1+\ln((r_{co}+r_{ci})/2r_{ci})/\lambda_2]}-\frac{2\Delta t\left(T_{2,j}^{0}-T_{3,j}^{0}\right)}{\rho_2C_2\left(r_{co}^2-r_{ci}^2\right)[\ln(2r_{co}/(r_{co}+r_{ci}))/\lambda_2+\ln((r_{co}+r_{b})/2r_{co})/\lambda_1]}-\frac{\lambda_2\Delta t\left(T_{2,j+1}^{0}-T_{2,j}^{0}+T_{2,j-1}^{0}\right)}{\rho_2C_2\Delta z^2} \tag{27}$$

The discretized form of the heat balance equation for the annulus fluid is:

$$T_{3,j}^{1}=T_{3,j}^{0}+\frac{2\Delta t\left(T_{2,j}^{0}-T_{3,j}^{0}\right)}{\rho_1C_1\left(r_b^2-r_{co}^2\right)[\ln(2r_{co}/(r_{co}+r_{ci}))/\lambda_2+\ln((r_b+r_{co})/2r_{co})/\lambda_1]}-\frac{2\Delta t\left(T_{2,j}^{0}-T_{3,j}^{0}\right)}{\rho_1C_1\left(r_b^2-r_{co}^2\right)\left[\ln(2r_b/(r_{co}+r_b))/\lambda_1+\ln\left(\left(r_{f1}+r_b\right)/2r_b\right)/\lambda_3\right]} \tag{28}$$

Table 1
Wellbore structure data.

Section	Casing procedure	Well depth, m	Wellbore diameter, mm	Casing outer diameter, mm	Casing inner diameter, mm
1	Surface casing	481	444.5	339.73	320.43
2	Technical casing	3287	311.1	244.48	224.16
3	Production casing	4572	212.73	168.28	151.52

Table 2
Thermophysical parameters of various materials.

Type	Density, g/cm^3	Specific heat capacity, J/(g·°C)	Thermal conductivity, W/(m·°C)
Drilling fluid	1.54	2.18	0.97
Spacer fluid	1.67	1.756	1.13
Cement slurry	1.91	1.38	1.47
Casing	7.8	0.4	46.0
Formation	2.64	0.837	2.65

Table 3
Rheological properties of various fluids.

Fluid type	Flow behavior index n	Consistency index k, Pa·S^n
Drilling fluid	0.64	0.29
Spacer fluid	0.63	0.35
Cement slurry	0.61	0.48

Table 4
Relevant parameters for temperature field calculation.

Parameter	Valve
Surface temperature	15.28 °C
Geothermal gradient	2.7 °C/100 m
Hydration exothermic rate of cement slurry	7.0 × 10^{-4} J/(g·s)

The discretized form of the heat balance equation for the wellbore wall is:

$$T_{4,j}^{1}=T_{4,j}^{0}+\frac{2\Delta t\left(T_{3,j}^{0}-T_{4,j}^{0}\right)}{\rho_3C_3\left(r_{\mathrm{f1}}^2-r_{\mathrm{b}}^2\right)\left[\ln(2r_{\mathrm{b}}/(r_{\mathrm{co}}+r_{\mathrm{b}}))\Big/\lambda_1+\ln\left(\left(r_{\mathrm{f1}}+r_{\mathrm{b}}\right)\Big/2r_{\mathrm{b}}\right)\Big/\lambda_3\right]}-\frac{2\Delta t\left(T_{2,j}^{0}-T_{3,j}^{0}\right)}{\rho_3C_3\left(r_{\mathrm{f1}}^2-r_{\mathrm{b}}^2\right)\left[\ln\left(\left(r_{\mathrm{f2}}+r_{\mathrm{f1}}\Big/\left(r_{\mathrm{b}}+r_{\mathrm{f1}}\right)\right)\Big/\lambda_3\right]}+\frac{\lambda_3\Delta t}{\rho_3C_3\Delta z^2}\left(T_{4,j+1}^{0}-2T_{4,j}^{0}+T_{4,j-1}^{0}\right) \tag{29}$$

The discretized form of the equation for the units inside the formation corresponds to Eq. (25).

Based on the above discretized equations, a numerical solution program for the temperature field has been developed to enable real-time calculation of the wellbore and formation temperature. The reliability of the model calculation results has been verified in previously published article (Feng et al., 2023).

3. Results and discussion

3.1. Basic data and cementing processes

(1) Basic data

Some thermal properties of the wellbore and formation materials are sourced from Holmes and Swift (1970) and Marshall and Bentsen (1982). The case well is a three-section vertical well, and its structure is detailed in Table 1. The thermal properties of various materials are listed in Table 2. The rheological properties of the fluids are provided in Table 3, where the displacement fluid is drilling fluid. Table 4 shows some other relevant parameters for temperature field calculation.

(2) Cementing processes

The entire cementing processes including sequential steps such as circulation flushing, pump stopping for wellbore preparation, pre-fluid injection, cement slurry injection, and displacement fluid injection. The detailed processes and parameters are shown in Table 5. During displacement, the drilling fluid temperature is higher than that during the circulation stage due to the increased temperature of the drilling fluid in the mud tanks from circulation. The pre-flush and displacement fluids are simplified as single fluids. The lead and tail slurries in the cement system are of the same type with identical density, differing only in the retarder concentration, resulting in similar thermal properties.

3.2. Analysis of initial temperature distribution during cementing

Based on the processes outlined in Table 5, the temperature

Table 5
Cementing processes and parameters.

Process	Fluid type	Injection temperature, °C	Injection rate, m^3/h	Time, s	Injection volume, m^3
Circulation flushing	Drilling fluid	23.89	47.69	32400	–
Wellbore preparation	Drilling fluid	–	–	5400	–
Pre-fluid injection	Spacer fluid	15.3	47.69	1500	19.87
Cement slurry 1 injection	Lead slurry	12.1	47.69	2800	37.09
Cement slurry 2 injection	Tail slurry	12.1	47.69	2000	26.50
Displacement fluid 1 injection	Drilling fluid	28.5	72	3822	76.44
Displacement fluid 2 injection	Drilling fluid	28.5	18	1200	6

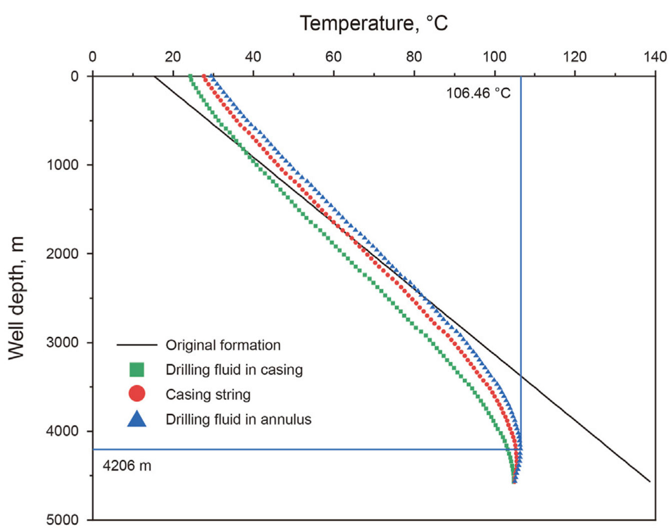

Fig. 6. Temperature distribution in the wellbore after 9 h (3 cycles) of circulation flushing.

distribution of the wellbore and surrounding formation is calculated sequentially. The wellbore circulation flushing and wellbore preparation stages are precursors to the cementing, and the temperature distribution at the start can be obtained through calculations of these stages.

3.2.1. Circulation flushing stage

The temperature distribution of the wellbore after 9 h of drilling fluid circulation, equivalent to three cycles, is shown in Fig. 6. The maximum temperature in the wellbore is 106.46 °C, located near a depth of 4206 m. The temperature of the fluid entering the wellbore is 24.32 °C at the wellhead, and the exit temperature is 29.54 °C.

3.2.2. Wellbore preparation stage

Following the circulation stage, wellbore preparations are made, including installing the cementing head, connecting pipelines, and pressure testing. During this time, the drilling fluid in the wellbore remains static for 90 min, resulting in the temperature distribution shown in Fig. 7(a). After 90 min of static drilling fluid, the maximum temperature of the annulus fluid is approximately 114.52 °C at the bottom of the well, while the maximum temperature of the casing fluid is approximately 108.44 °C, with a temperature difference of about 6.08 °C between the two. At the wellhead, the temperature of the drilling fluid in the casing is 25.41 °C, while the temperature in the annulus is 24.75 °C. The drilling fluid in the annulus cools significantly due to heat transfer with the surrounding formation.

The temperature distribution at different distances from the annulus in the formation is analyzed in Fig. 7(b). Before the cementing process begins, it is evident that the temperature distribution of the formation near the wellbore has already changed significantly compared to the original formation temperature. The temperature of the formation within a radius of 0.8 m from the wellbore has decreased in the lower part of the well, while the temperature in the upper part has increased.

3.3. Temperature analysis during cementing processes

The cementing process generally includes pumping spacer fluid, cement slurry, and displacement fluid. Based on the initial temperature distribution (Fig. 7) of the wellbore and formation at the

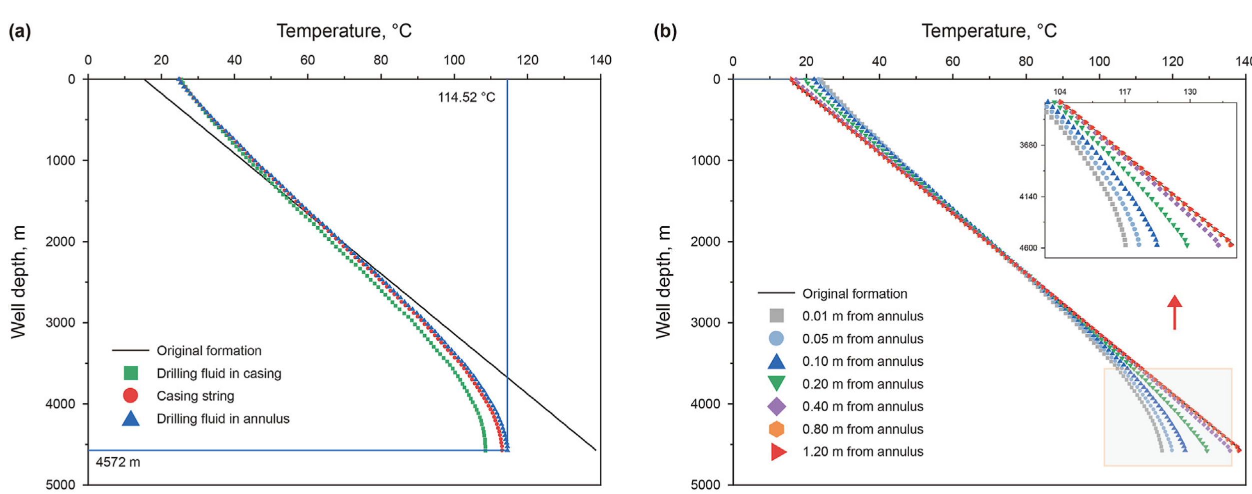

Fig. 7. Temperature distribution after 90 min of fluid static conditions. (**a**) wellbore temperature, (**b**) formation temperature.

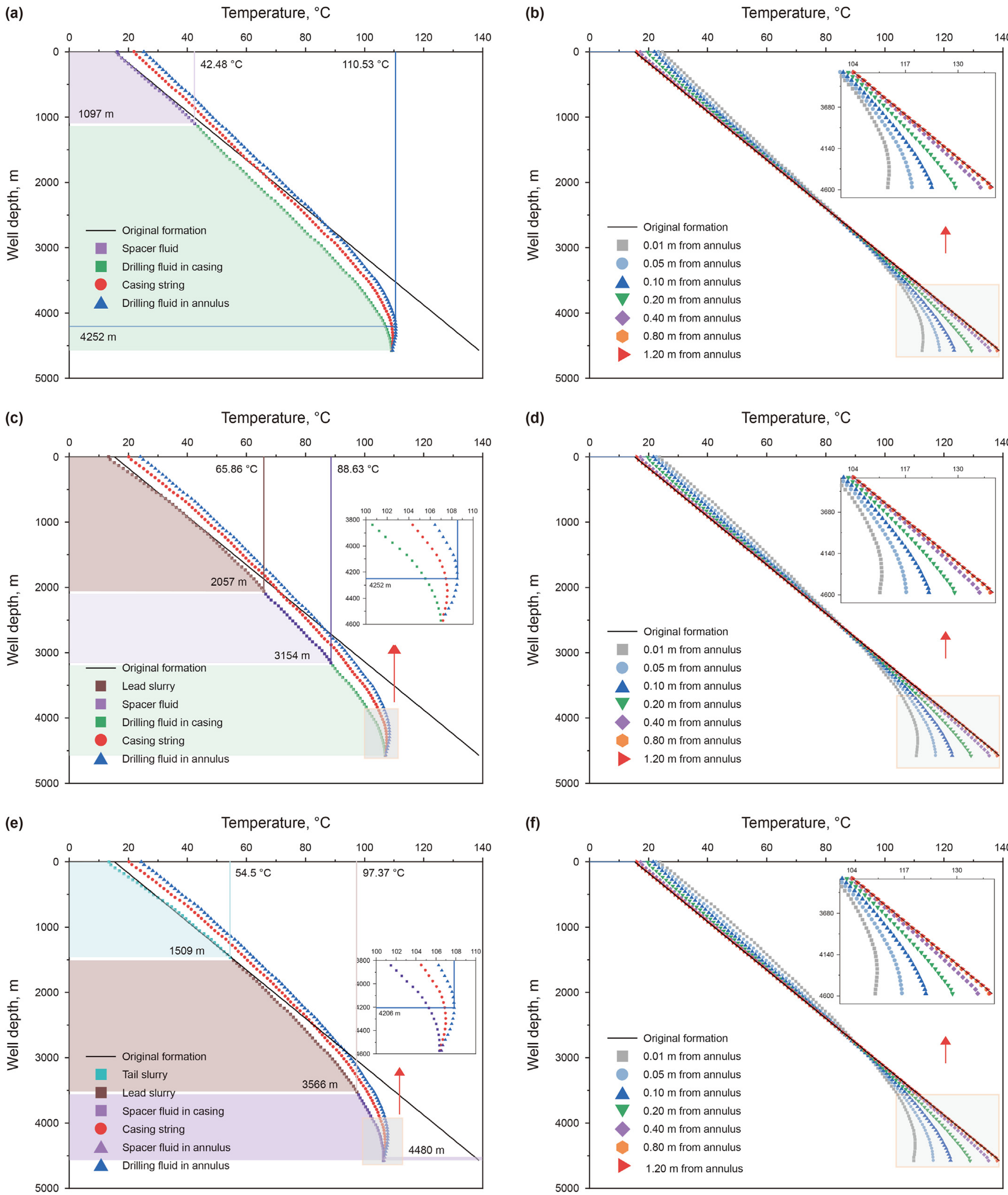

Fig. 8. Temperature distribution of multi-fluid injection (left: wellbore temperature, right: formation temperature). (**a**–**b**) spacer fluid injection, (**c**–**d**) lead slurry injection, (**e**–**f**) tail slurry injection.

start of the process, the temperature changes during each stage are calculated, along with the BHCT of the cement slurry.

3.3.1. Spacer fluid injection stage

After the spacer fluid is injected, the temperature distribution of the fluids and casing in the wellbore is shown in Fig. 8(a). The injection temperature of the spacer fluid is 16.17 °C, and the return temperature of the drilling fluid at the wellhead is 25.24 °C. Compared to the circulation stage (Fig. 6), the exit temperature has decreased by 4.3 °C. Since the spacer fluid is cooler than the drilling fluid, the cooling effect is more pronounced. The maximum temperature in the wellbore is 110.53 °C, located near 4252 m in the annulus. The temperature distribution of the spacer fluid ranges from 16.17 to 42.48 °C, corresponding to a depth of 0–1097 m in the casing.

The temperature distribution in the formation after spacer fluid injection is shown in Fig. 8(b). At a distance of 0.01 m from the annulus, the formation temperature at the wellhead is 24.68 °C. Compared to the end of the wellbore preparation stage (Fig. 7), where the temperature was 24.17 °C, the temperature has increased by 0.51 °C, while the maximum temperature at the bottom of the well (around a depth of 4389 m) has decreased by 4.14–112.88 °C.

3.3.2. Cement slurry injection stage

(1) Pumping the lead slurry

After injecting 37.09 m^3 of lead slurry, the temperature distribution in the wellbore is shown in Fig. 8(c). Currently, three fluids are present in the wellbore: drilling fluid, spacer fluid, and cement slurry. The injection temperature of the lead slurry is 13.3 °C, and the return temperature of the drilling fluid at the wellhead is 24.11 °C, a decrease of 1.13 °C compared to the end of the spacer fluid injection. The lead slurry occupies a length of 2057 m, with a temperature range of 13.3–65.86 °C. The maximum temperature in the wellbore is located at a depth of approximately 4252 m, with a temperature of 108.55 °C. Compared to the end of the spacer fluid injection, the maximum temperature in the wellbore has further decreased.

The temperature distribution in the formation after lead slurry injection is shown in Fig. 8(d). At a distance of 0.01 m from the annulus, the maximum temperature at a depth of approximately 4343 m is 111.05 °C, while the temperature at the wellhead is 23.69 °C. Compared to the end of the spacer fluid injection, the near-wellbore formation temperature from the wellhead to the bottom of the well has decreased.

Generally, the longer the fluid circulation time, the lower the temperature in the lower section of the wellbore annulus fluid and the surrounding area (typically within a radial distance of 1 m), eventually stabilizing. Meanwhile, the fluid outlet temperature and the temperature of the surrounding formation in the upper section of the wellbore will increase. This behavior aligns with the general pattern of changes in the fluid circulation temperature field. However, after lead slurry injection, the temperature of the drilling fluid returning to the wellhead and the temperature of the formation near the wellbore both decrease. This is because the injection temperature of the lead slurry is lower than that of both the spacer fluid and drilling fluid, and heat convection removes more heat from the annulus fluid, reducing the temperature of the casing, annulus fluid, and the surrounding formation.

The temperature changes in the surrounding formation in the upper section of the wellbore during cementing are complex. Typically, the temperature of the annulus fluid is higher than that of the adjacent formation, so the temperature of the near-annulus formation is higher than that of the distant formation. The near-formation continuously transfers heat to the distant formation through conduction. As the operation proceeds, the temperature of the distant formation continues to rise. The temperature of the surrounding formation will be influenced by the temperature of the injected fluids. When the temperature of the injected fluids decreases significantly, heat convection can reduce the temperature of the adjacent annulus fluid. If the heat gained by the near-wellbore formation from convective heat transfer with the annulus fluid is less than the heat loss through radial heat conduction, the temperature of the near-wellbore formation will temporarily decrease. As fluid circulation continues, the temperature of the annulus fluid rises (increasing the exit temperature), increasing the heat gained by the near-wellbore formation through convective heat transfer, and the temperature will rise accordingly.

(2) Pumping the tail slurry

After injecting 26.50 m^3 of tail slurry, the temperature distribution of the fluids and casing in the wellbore is shown in Fig. 8(e). The fluids in the wellbore include drilling fluid, spacer fluid, lead slurry, and tail slurry. The temperature distribution of the fluids is as follows: the drilling fluid is distributed above 4480 m in the annulus, with a temperature range of 24.32–107.81 °C; the spacer fluid is distributed between 4480 and 4572 m in the annulus, with a temperature range of 106.56–106.69 °C, and between 3566 and 4572 m in the casing, with a temperature range of 97.87–106.32 °C; the lead slurry is distributed between 1509 and 3566 m in the casing, with a temperature range of 55.56–97.37 °C; and the tail slurry is distributed above 1509 m in the casing, with a temperature range of 13.32–54.50 °C. The temperature of the returning drilling fluid at the wellhead has increased by 0.21 °C compared to the end of the lead slurry injection, while the maximum temperature in the wellbore (located at a depth of approximately 4206 m) has decreased by 0.74 °C.

The temperature distribution in the surrounding formation is shown in Fig. 8(f). Compared to the end of the lead slurry injection, the temperature in the lower part of the formation has further decreased, while the temperature at the wellhead has increased. At a distance of 0.01 m from the annulus, the maximum temperature at the bottom is 110.18 °C, a decrease of 0.87 °C compared to the end of the lead slurry injection, and the temperature at the wellhead is 23.77 °C, an increase of 0.08 °C.

3.3.3. Displacement fluid injection stage

In typical cementing processes, the displacement of drilling fluid and spacer fluid from the annulus by cement slurry occurs in two stages. Initially, a high displacement rate is employed to displace

Table 6
Division of high-rate displacement stage.

Stage	Process	Fluid type	Injection temperature, °C	Rate, m^3/h	Time, s	Volume, m^3
1	Lead slurry returns to 4200 m	Drilling fluid	28.5	72	1190	23.80
2	Tail slurry returns to 4200 m	Drilling fluid	28.5	72	1854.6	37.09
3	High-rate displacement ends	Drilling fluid	28.5	72	777.4	15.55

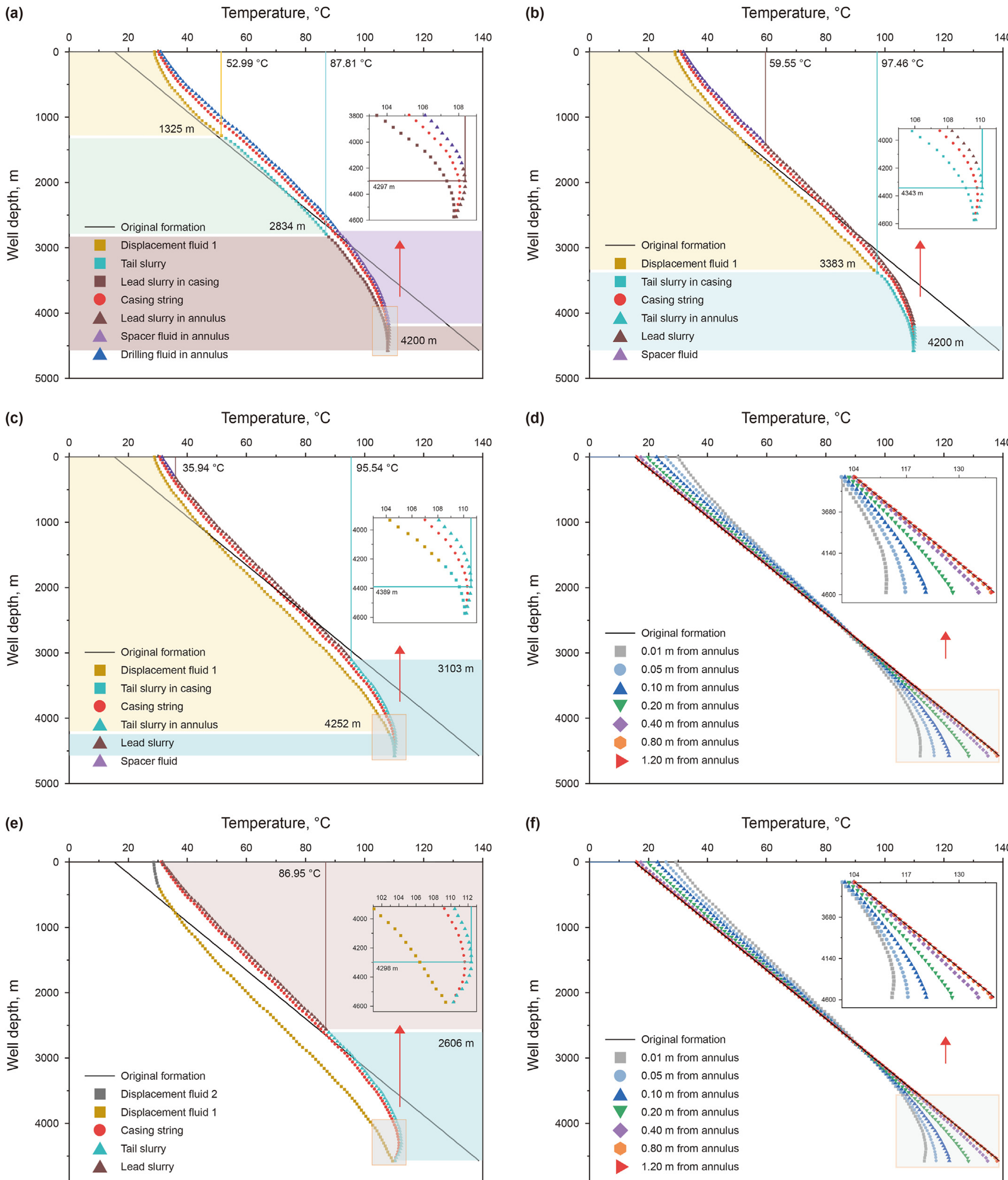

Fig. 9. Temperature distribution of displacement fluid injection. (**a**) lead slurry returns to 4200 m, (**b**) tail slurry returns to 4200 m, (**c**) high-rate displacement ends, (**d**) formation temperature after high-rate displacement, (**e**) low-rate displacement ends, (**f**) formation temperature after low-rate displacement.

most of the cement slurry into the annulus, followed by a lower rate with a smaller volume of displacement fluid to ensure careful displacement and secure pressure bumping, as shown in Table 5.

(1) High-rate displacement stage

From the previous analysis, it is evident that the temperature hotspot within the wellbore is located at a depth of approximately 4200 m. While the hotspot depth may vary due to multiple factors, it generally remains relatively stable as long as the well depth and structure remain unchanged (Wang et al., 2022). Based on this, it can be inferred that the maximum temperature of the lead and tail cement slurries will likely occur near this 4200 m depth. To better analyze the maximum circulation temperature of the lead and tail slurries, the high-rate displacement process is further subdivided into three stages, as shown in Table 6.

1) High-rate displacement stage 1

During this stage, the front of the lead slurry returns to a height of 4200 m. The temperature distribution in the wellbore is shown in Fig. 9(a). The fluids present in the wellbore include drilling fluid, spacer fluid, lead slurry, tail slurry, and displacement fluid 1. The lead slurry is distributed in the annulus between 4200 and 4572 m, with temperatures ranging from 107.87 to 108.36 °C. Inside the casing, the lead slurry is distributed between depths of 2834 and 4752 m, with temperatures ranging from 87.81 to 107.73 °C. The tail slurry is distributed within the casing between depths of 1325 and 2834 m, with temperatures ranging from 52.99 to 86.85 °C.

2) High-rate displacement stage 2

In this stage, the front of the tail slurry returns to a height of 4200 m, as shown in Fig. 9(b). The lead slurry is distributed in the annulus between 1417 and 4200 m, with temperatures ranging from 59.55 to 109.77 °C. The tail slurry is distributed in the annulus between 4200 and 4572 m, with temperatures ranging from 109.92 to 110.14 °C, and inside the casing between 3383 and 4572 m, with temperatures ranging from 97.46 to 109.61 °C. The hotspot temperature is located at a depth of approximately 4343 m, with a temperature of 110.14 °C. Therefore, it can be concluded that the maximum circulation temperature of the lead slurry during this process is approximately 109.92 °C.

3) High-rate displacement stage 3

The temperature distribution in the wellbore during this stage is shown in Fig. 9(c). The lead slurry is distributed in the annulus between 320 and 3103 m, with temperatures ranging from 35.94 to 94.69 °C. The tail slurry is distributed in the annulus between 3103 and 4572 m, with temperatures ranging from 95.54 to 110.56 °C, and inside the casing between depths of 4252 and 4572 m, with temperatures ranging from 108.58 to 110.07 °C. The hotspot temperature in the wellbore is 110.56 °C, located at a depth of approximately 4389 m. Compared to stage 2, the hotspot temperature has increased by 0.42 °C, and the hotspot has moved closer to the bottom of the well, shifting downward by approximately 46 m. The displacement rate is indeed a critical factor influencing the depth of the hotspot (Wang et al., 2022).

The temperature distribution of the surrounding formation is shown in Fig. 9(d). The temperature of the formation near the bottom of the well has increased, while the temperature of the formation farther from the annulus has continued to decrease. The temperature near the wellhead has also increased. Analyzing the temperature at a distance of 0.01 m from the annulus, the maximum temperature at the bottom of the well is 111.97 °C, which is 1.79 °C higher than that after the tail slurry was injected. At the wellhead, the temperature has increased by 6.17 °C. At a distance of 0.4 m from the annulus, the maximum temperature at the bottom of the well is 134.80 °C, compared to 135.08 °C previously, a decrease of 0.28 °C. The wellhead temperature has increased from 17.28 to 17.36 °C.

The increase in the fluid hotspot temperature and the temperature of the near-wellbore formation during the displacement stage is due to the higher temperature of the displacement fluid compared to the cement slurry and spacer fluid. Additionally, the heat generated by cement slurry hydration and friction further raises the wellbore temperature. Once the wellbore temperature rises, the heat exchange between the wellbore and the formation near the bottom of the well decreases. Continuous heat conduction in the formation farther from the wellbore results in a gradual recovery of the wellbore temperature. However, the temperature in the formation farther from the wellbore (e.g., at a distance greater than 0.4 m from the annulus) continues to decrease. The temperature of the annulus fluid at the wellhead rises rapidly due to the increased temperature of the fluid injected into the casing, causing the surrounding temperature to rise.

(2) Low-rate displacement stage

At a low displacement rate of 18 m^3/h, displacement was completed and pressure bumping was performed to conclude the cementing processes. Upon completion of displacement, the cement slurry returned to the design depth, fully occupying the annulus space, while the displacement fluid filled the casing, as shown in Fig. 9(e).

At the end of the cementing processes, the temperature distribution of the lead slurry ranged from 31.58 to 86.95 °C in the interval between 0 and 2606 m, while the tail slurry temperature ranged from 87.91 to 112.38 °C in the interval between 2606 and 4572 m. Compared to the high-rate displacement stage, the temperature of the fluids in the wellbore has further increased, with a hotspot temperature of 112.38 °C at a depth of approximately 4298 m, representing an increase of 1.82 °C. With lower displacement rates, the fluid has more time to exchange heat through convection, thereby absorbing more heat from the formation and increasing its temperature.

The temperature distribution in the surrounding formation at the end of the cementing processes is shown in Fig. 9(f). Compared to the previous stage, the temperature of the formation near the wellbore has increased further. The temperature of the formation farther from the annulus increased gradually in the upper sections of the well but decreased slowly in the lower sections.

Through the above calculations and analysis, the axial temperature distribution of the cement slurry and the BHCT were obtained. After the cement slurry reached the design location, the temperature of the lead slurry ranged from 31.58 to 86.95 °C. During the entire flow process, the BHCT of the lead slurry was 109.92 °C, while the tail slurry temperature ranged from 87.91 to 112.38 °C, with the BHCT of 112.38 °C. Under conventional cementing displacement techniques and working fluid column structures, the BHCT of the cement slurry is higher than the temperature during drilling fluid circulation (Fig. 6), with the BHCT of the tail slurry being higher than that of the lead slurry.

3.4. Influence of initial temperature on cement slurry BHCT

Previous studies on cement slurry BHCT often do not consider the circulation flushing and wellbore preparation steps. Generally, the calculation begins by assuming that the wellbore is filled with

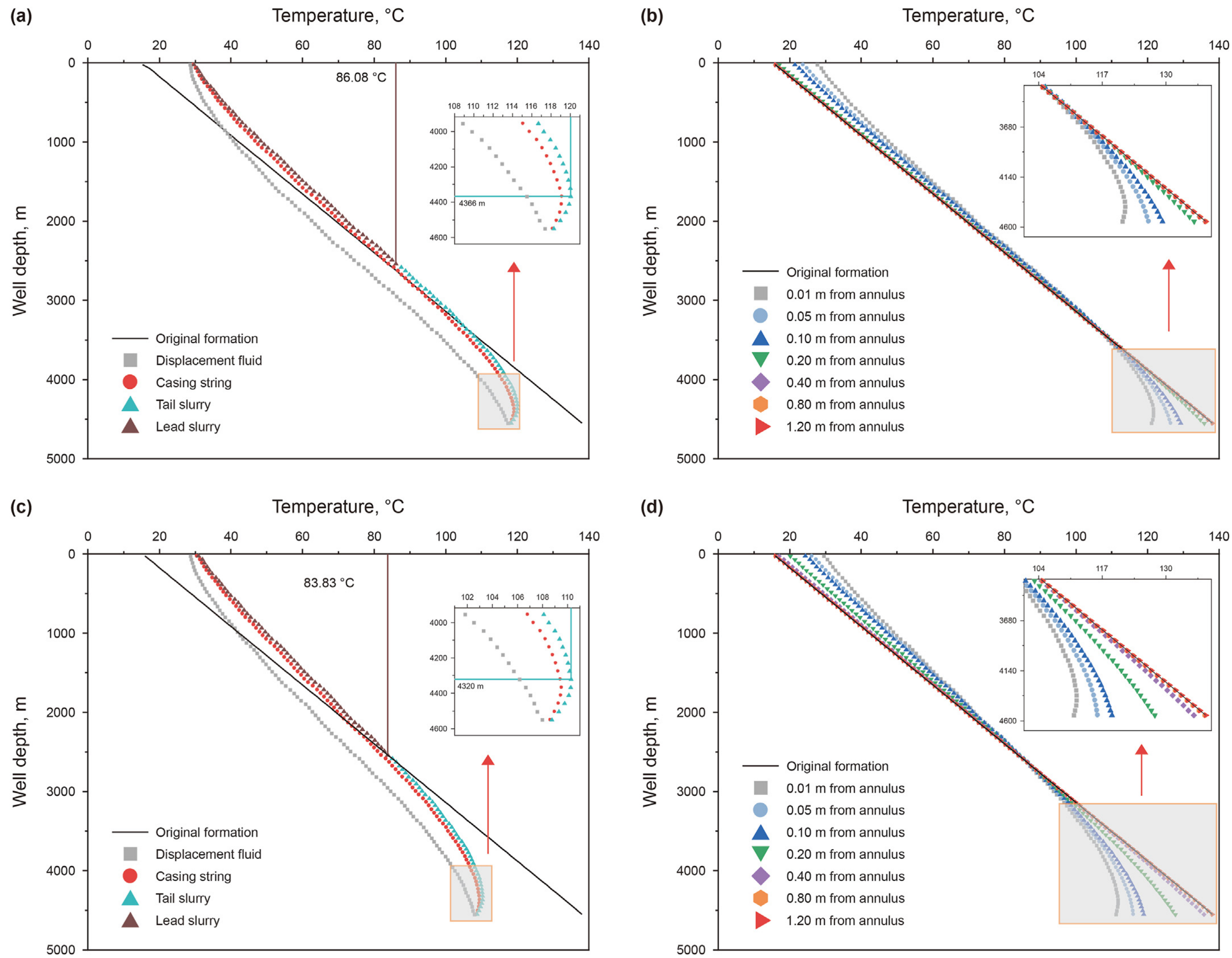

Fig. 10. Temperature distribution of cementing processes (left: wellbore temperature, right: formation temperature). (**a**–**b**) not considering circulation flushing, (**c**–**d**) not considering wellbore preparation.

drilling fluid, and the temperature distribution of both the wellbore and the formation is identical to the original formation temperature.

3.4.1. *Not considering circulation flushing*

When the circulation flushing stage is ignored, the temperature distribution of the wellbore and formation during the cementing processes is assumed to match the original formation temperature. Fig. 10(a) shows the wellbore temperature distribution at the end of cementing processes without considering circulation flushing. The lead slurry occupies the depth from 0 to 2606 m with temperatures ranging from 29.58 to 86.08 °C, while the tail slurry occupies the depth from 2606 to 4572 m with temperatures ranging from 87.52 to 120.02 °C. The drilling fluid occupies the depth from 0 to 4572 m with temperatures ranging from 28.58 to 117.36 °C. Compared to the wellbore temperature in actual cementing processes (Fig. 9), the hotspot temperature of the tail slurry is overestimated by 7.64 °C, and the temperature of the lead slurry returning to the surface is underestimated by 2.0 °C.

Fig. 10(b) shows the formation temperature distribution around the wellbore at the end of cementing processes. Due to the short displacement time, the radial temperature impact range is within 0.4 m. Compared to the formation temperature during actual cementing processes (Fig. 9), the temperature near the wellbore in the lower section of the well is higher, while it is lower in the upper section. For example, at a distance of 0.01 m from the annulus, the maximum temperature at the bottom of the well is 121.60 °C, which is 7.80 °C higher than in actual processes. However, at the wellhead, the temperature is 27.72 °C, which is 1.46 °C lower.

If the circulation flushing step is ignored, the initial temperature distribution of the wellbore and surrounding formation at the start of the cementing processes are equal to the original formation temperature. As a result, the temperature in the lower section of the wellbore is too high, and the temperature in the upper section is too low. Consequently, the calculated BHCT of the cement slurry is overestimated, while the temperature of the fluid returning to the surface is underestimated.

3.4.2. *Not considering wellbore preparation*

When the wellbore preparation stage is ignored, the initial temperature distribution in the wellbore at the start of cementing corresponds to that shown in Fig. 6. The wellbore temperature distribution at the end of cement slurry displacement is shown in Fig. 10(c). The lead slurry occupies the depth from 0 to 2606 m, with temperatures ranging from 30.95 to 83.83 °C. The tail slurry occupies the depth from 2606 to 4572 m, with temperatures ranging from 85.06 to 110.28 °C. The drilling fluid inside the casing has temperatures ranging from 28.67 to 107.99 °C. Compared to the wellbore temperature in actual cementing processes, the hotspot temperature of the cement slurry is underestimated by 2.1 °C.

Fig. 10(d) shows the formation temperature distribution around the wellbore at the end of cementing processes. Compared to actual cementing processes, the temperature in the lower section of the well is lower. For example, at a distance of 0.01 m from the annulus, the maximum temperature at the bottom of the well is 111.69 °C, which is 2.11 °C lower. When the wellbore preparation step is ignored, the temperature in the lower section of the wellbore does not adequately recover, resulting in a lower calculated BHCT for the cement slurry compared to actual processes.

4. Conclusion

A comprehensive temperature field model for the entire cementing process was established. This model enables the numerical calculation of wellbore and formation temperatures throughout circulation flushing, wellbore preparation, and cement slurry injection. It includes real-time tracking calculations of the location and temperature of each fluid and the temperature distribution at different locations in the formation surrounding the annulus.

(1) The calculation of cement slurry BHCT was achieved under the consideration of multiple cementing processes steps and various working fluids. The BHCT value changes continuously during the cementing processes, indicating it is a transient parameter.
(2) The BHCT for the lead slurry and tail slurry are not identical during cementing processes. In this study, the maximum BHCT of the tail slurry was 2.46 °C higher than that of the lead slurry. Therefore, the difference between the two should be considered when designing the cement slurry formulation.
(3) Ignoring circulation flushing and wellbore preparation from the cementing processes can lead to errors in the calculated cement slurry BHCT. In this study, ignoring the circulation flushing stage resulted in an overestimation of the BHCT by 7.64 °C, while ignoring the wellbore preparation stage led to an underestimation of the BHCT by 2.1 °C.
(4) Traditional API methods for predicting cement slurry BHCT obtains the recommended empirical chart or calculation formula by summarizing the circulating temperature of drilling fluid. However, drilling operation conditions and cementing processes are significant different, and their BHCT values are not the same. The BHCT of cement slurry is influenced by a combination of factors, including the previous processes stages, the thermal properties of fluids in the wellbore, the wellbore structure, and the cementing process. The recommendation algorithm of cement slurry BHCT at the oilfield site needs to be improved.

CRediT authorship contribution statement

Xu-Ning Wu: Writing – review & editing, Writing – original draft, Formal analysis, Conceptualization. **Zheng-Meng Hou:** Writing – review & editing, Supervision, Project administration. **Zao-Yuan Li:** Writing – review & editing, Visualization, Funding acquisition. **Bo Feng:** Writing – original draft, Methodology, Investigation, Data curation. **Lin Wu:** Methodology, Formal analysis. **Qian-Jun Chen:** Visualization, Formal analysis. **Nan Cai:** Investigation. **Ting-Cong Wei:** Investigation, Formal analysis.

Data availability

Data will be made available on request.

Declaration of competing interests

The authors declare that they have no known competing financial interests or personal relationships that could have appeared to influence the work reported in this paper.

Acknowledgments

This work was supported by the National Natural Science Foundation of China (No. U22B6003 and No. 52274010) and the China Scholarship Council (No. 202008080235).

References

Abdelhafiz, M.M., Hegele, L.A., Oppelt, J.F., 2020. Numerical transient and steady state analytical modeling of the wellbore temperature during drilling fluid circulation. J. Pet. Sci. Eng. 186, 106775. https://doi.org/10.1016/j.petrol.2019.106775.
Abdelhafiz, M.M., Hegele, L.A., Oppelt, J.F., 2021. Temperature modeling for wellbore circulation and shut-in with application in vertical geothermal wells. J. Pet. Sci. Eng. 204, 108660. https://doi.org/10.1016/j.petrol.2021.108660.
Arnold, F.C., 1990. Temperature variation in a circulating wellbore fluid. J. Energy Resour. Technol. 112, 79–83. https://doi.org/10.1115/1.2905726.
Beirute, R.M., 1991. A circulating and shut-in well-temperature-profile simulator. J. Petrol. Technol. 43, 1140–1146. https://doi.org/10.2118/17591-PA.
Bird, R.B., Lightfoot, E.N., Stewart, W.E., 1960. Solutions to the Class 1 and Class 2 Problems in Transport Phenomena. Wiley.
Bittleston, S.H., 1990. A two-dimensional simulator to predict circulating temperatures during cementing operations. In: SPE Annual Technical Conference and Exhibition. New Orleans, Louisiana. https://doi.org/10.2118/20448-MS.
Chen, Z., Novotny, R.J., 2003. Accurate prediction wellbore transient temperature profile under multiple temperature gradients: finite difference approach and case history. In: SPE Annual Technical Conference and Exhibition, Denver, Colorado. https://doi.org/10.2118/84583-MS.
Davies, S.N., Gunningham, M.M., Bittleston, S.H., et al., 1994. Field studies of circulating temperatures under cementing conditions. SPE Drill. Complet. 9, 12–16. https://doi.org/10.2118/21973-PA.
Edwardson, M.J., Girner, H.M., Parkison, H.R., et al., 1962. Calculation of formation temperature disturbances caused by mud circulation. J. Petrol. Technol. 14, 416–426. https://doi.org/10.2118/124-PA.
Feng, B., Li, J., Li, Z., et al., 2023. Enhancing environmental protection in oil and gas wells through improved prediction method of cement slurry temperature. Energies 16 (13), 4852. https://doi.org/10.3390/en16134852.
Garcia, J.A., Clark, C.R., 1976. An investigation of annular gas flow following cementing operations. In: SPE Symposium on Formation Damage Control, Houston, Texas, p. 5701. https://doi.org/10.2118/5701-MS.
Guillot, F., Boisnault, J.M., Hujeux, J.C., 1993. A cementing temperature simulator yo improve field practice. In: SPE/IADC Drilling Conference, Amsterdam, Netherlands. https://doi.org/10.2118/25696-MS.
Guo, S., Bu, Y., Liu, H., et al., 2014. The abnormal phenomenon of class g oil well cement endangering the cementing security in the presence of retarder. Constr. Build. Mater. 54, 118–122. https://doi.org/10.1016/j.conbuildmat.2013.12.057.
Guo, S., Bu, Y., Lu, Y., 2019. Addition of tartaric acid to prevent delayed setting of oil-well cement containing retarder at high temperatures. J. Pet. Sci. Eng. 172, 269–279. https://doi.org/10.1016/j.petrol.2018.09.053.
Holmes, C.S., Swift, S.C., 1970. Calculation of circulating mud temperatures. J. Petrol. Technol. 22, 670–674. https://doi.org/10.2118/2318-PA.
Honore, R.S., Tarr, B.A., Howard, J.A., et al., 1993. Cementing temperature predictions based on both downhole measurements and computer predictions: a case history. In: SPE Production Operations Symposium, Oklahoma City, Oklahoma. https://doi.org/10.2118/25436-MS.
Kabir, C.S., Hasan, A.R., Kouba, G.E., et al., 1996. Determining circulating fluid temperature in drilling, workover, and well control operations. SPE Drill. Complet. 11, 74–79. https://doi.org/10.2118/24581-PA.
Keller, H.H., Couch, E.J., Berry, P.M., 1973. Temperature distribution in circulating mud columns. Soc. Petrol. Eng. J. 13, 23–30. https://doi.org/10.2118/3605-PA.
Mangadlao, J.D., Cao, P., Advincula, R.C., 2015. Smart cements and cement additives for oil and gas operations. J. Pet. Sci. Eng. 129, 63–76. https://doi.org/10.1016/j.petrol.2015.02.009.
Marshall, D.W., Bentsen, R.G., 1982. A computer model to determine the temperature distributions in a wellbore. J. Can. Petrol. Technol. 21 (1). https://doi.org/

10.2118/82-01-05.
Moss, J.T., White, P.D., 1959. How to calculate temperature profiles in a water-injection well. Oil Gas J. 57, 174.
Petukhov, B.S., 1970. Heat transfer and friction in turbulent pipe flow with variable physical properties. In: Hartnett, J.P., Irvine, T.F. (Eds.), Advances in Heat Transfer. Elsevier, pp. 503–564. https://doi.org/10.1016/S0065-2717(08)70153-9.
Ramey, H.J., 1962. Wellbore heat transmission. J. Petrol. Technol. 14, 427–435. https://doi.org/10.2118/96-PA.
Raymond, L.R., 1969. Temperature distribution in a circulating drilling fluid. J. Petrol. Technol. 21, 333–341. https://doi.org/10.2118/2320-PA.
Sump, G.D., Williams, B.B., 1973. Prediction of wellbore temperatures during mud circulation and cementing operations. J. Eng. Industry 95, 1083–1092. https://doi.org/10.1115/1.3438255.
Wang, C., Liu, H., Yu, G., et al., 2024. Wellbore-heat-transfer-model-based optimization and control for cooling downhole drilling fluid. Pet. Sci. 21 (3), 1955–1968. https://doi.org/10.1016/j.petsci.2023.11.025.
Wang, R., Kuru, E., Yan, Y., et al., 2022. Sensitivity analysis of factors controlling the cement hot spot temperature and the corresponding well depth using a combined cfd simulation and machine learning approach. J. Pet. Sci. Eng. 208, 109617. https://doi.org/10.1016/j.petrol.2021.109617.
Wang, R., Kuru, E., Yang, X., et al., 2021. Prediction of transient wellbore cement circulating temperature distribution using cfd simulation. J. Pet. Sci. Eng. 196, 107912. https://doi.org/10.1016/j.petrol.2020.107912.
Wang, R., Wang, Y., Tyagi, M., et al., 2019. Multi-dimensional cfd analysis for the prediction of transient wellbore circulating temperature profile to guide offshore cementing job. J. Korean Soc. Mineral and Energy Res. Engineers 56, 344–358. https://doi.org/10.32390/ksmer.2019.56.4.344.
Wu, J., Han, R.D., 2009. A new approach to predicting the maximum temperature in dry drilling based on a finite element model. J. Manuf. Process. 11, 19–30. https://doi.org/10.1016/j.jmapro.2009.07.001.
Yang, M., Li, X., Deng, J., et al., 2015. Prediction of wellbore and formation temperatures during circulation and shut-in stages under kick conditions. Energy 91, 1018–1029. https://doi.org/10.1016/j.energy.2015.09.001.
Yang, M., Luo, D., Chen, Y., et al., 2019. Establishing a practical method to accurately determine and manage wellbore thermal behavior in high-temperature drilling. Appl. Energy 238, 1471–1483. https://doi.org/10.1016/j.apenergy.2019.01.164.
Yang, M., Zhao, X., Meng, Y., et al., 2017. Determination of transient temperature distribution inside a wellbore considering drill string assembly and casing program. Appl. Therm. Eng. 118, 299–314. https://doi.org/10.1016/j.applthermaleng.2017.02.070.
Zhang, Y., Li, Y., Kong, X., et al., 2024. Temperature prediction model in multiphase flow considering phase transition in the drilling operations. Pet. Sci. 21 (3), 1969–1979. https://doi.org/10.1016/j.petsci.2024.01.004.
Zhang, Z., Xiong, Y., Gao, Y., et al., 2018. Wellbore temperature distribution during circulation stage when well-kick occurs in a continuous formation from the bottom-hole. Energy 164, 964–977. https://doi.org/10.1016/j.energy.2018.09.048.